J Mater Sci (2014) 49:633–641
DOI 10.1007/s10853-013-7743-5

Mixed-valence $La_{0.80}(Ag_{1-x}Sr_x)_{0.20}MnO_3$ manganites with magnetocaloric effect

M. E. Amano · I. Betancourt · J. L. Sánchez Llamazares · L. Huerta · C. F. Sánchez-Valdés

Received: 31 May 2013 / Accepted: 13 September 2013 / Published online: 24 September 2013

Abstract We report the effect of the simultaneous inclusion of Ag^{1+} and Sr^{2+} cations on the crystal structure and the magnetocaloric effect (MCE) of $La_{0.80}(Ag_{1-x}Sr_x)_{0.20}MnO_3$ manganites ($x = 0.0$, 0.25, 0.50, 0.75, 1.0) synthesized by the solid-state reaction method. X-ray photoelectron spectroscopy was used to verify chemical composition and the amount of Mn^{3+}–Mn^{4+} cations, while the magnetic performance was evaluated by means of a Physical Property Measuring System. The progressive substitution of Ag^{1+} by Sr^{2+} causes the increase of the number of Mn^{4+} cations, together with increasing ionic radii for the A-site contents up to $x = 0.75$, both favoring the enhancement of the double-exchange interaction and hence, the MCE. Excellent values of magnetic entropy change (−4.6 J/kg K, $\mu_o\Delta H = 5.0$ T) were observed for the $x = 0.25$ manganite, while for the $x = 0.50$ sample interesting refrigerant capacity (129 J/kg, $\mu_o\Delta H = 2.0$ T) and a wide interval of temperature at the full-width at half maximum δT_{FWHM} of the magnetic entropy change curve were recorded (101 K, $\mu_o\Delta H = 2.0$ T) caused by two successive magnetic transitions. Magnetic performance was explained in terms of the effect of the cation substitution on the double-exchange interaction and the tolerance factor.

M. E. Amano · I. Betancourt (✉) · L. Huerta
Departamento de Materiales Metálicos y Cerámicos, Instituto de Investigaciones en Materiales, Universidad Nacional Autónoma de México, 04510 Mexico, DF, Mexico
e-mail: israelb@unam.mx

J. L. Sánchez Llamazares
Instituto Potosino de Investigación Científica y Tecnológica, Camino a la Presa San José 2055, Col. Lomas 4a, 78216 San Luis Potosí, SLP, Mexico

C. F. Sánchez-Valdés
Institut de Ciencia de Materials de Barcelona (C.S.I.C.), Campus U.A.B., 08193 Bellaterra, Spain

Introduction

The magnetocaloric effect (MCE) refers to the isothermal magnetic entropy change (or the temperature change under adiabatic conditions) of a magnetic material under the application of an external magnetic field change $\mu_o\Delta H$. This phenomenon is known since 1881, however, it was not up to the 1930s, that it was used for reaching ultra-low temperatures (i.e., $\ll 1$ K) by means of the adiabatic demagnetization of paramagnetic salts like $Gd_2(SO_4)_3{\cdot}8H_2O$ [1]. The MCE has recently elicited a renewed interest due to the possibility of developing magnetic refrigeration technology applicable at room temperature, with the expectation of achieving higher cooling efficiencies (over 50 % of a Carnot cycle, [2–4]), compared with conventional refrigeration based on gas compression of pollutant compounds like CFC. One of the figures of merit for materials characterization aiming to MCE applications is the variation of the magnetic entropy ΔS_M for a given applied magnetic field change $\mu_o\Delta H = \mu_o(H_f - H_i)$ (where $\mu_o H_i$ is usually zero). In adiabatic conditions, the decrease (increase) of the magnetic entropy due to the application (removal) of the magnetic field leads to the increase (decrease) of the lattice entropy giving rise to a temperature increment (decrement) of the material. An additional parameter for MCE characterization is the refrigerant capacity (RC), which measures the ability of the magnetic refrigerant to transfer thermal energy between the cold (T_{cold}) and hot (T_{hot}) sinks when an ideal thermodynamic cycle is considered. To date, the reference material for MCE applications at room temperature is pure Gd, which possesses the most promising

combination of properties for magnetic refrigeration applications at room temperature: ΔS_M of -10.2 J/kg K ($\mu_o\Delta H = 5$ T), RC of 410 J/kg, and $T_C = 294$ K [4] alongside an adiabatic temperature change ΔT_{ad} of 6.0 K for $\mu_o\Delta H = 2$ T [5]. Unfortunately, the considerable high price and cost of production (USD $4000/kg [4]), makes Gd a disadvantageous choice as magnetic refrigerant. Because of this, a wide variety of materials have been explored for MCE applications, including MnFePAs alloys (with ΔS_M as high as -18 J/kg K $\mu_o\Delta H = 5$ T and $T_C = 308$ K [6]), MnFePAsGe alloys (with ΔS_M of up to -40 J/kg K, $\mu_o\Delta H = 3$ T, $T_C = 270$ K [7]) Heusler alloys like NiMnGa (with ΔS_M of up to -10.4 J/kg K, $\mu_o\Delta H = 2$ T, and $RC = 47$ J/kg [8], NiMnCoSn (with $\Delta S_M = -30$ J/kg K, $\mu_o\Delta H = 1$ T, $T_C = 271$ K and RC $\sim$ 44 J/kg [9]), or NiMnIn with structural and magnetic entropy changes between -2.6 and -7.2 J/kg K, $\mu_o\Delta H = 3$ T and RC between 60 and 95 J/kg [10], rare earth-based bulk metallic glasses, like GdAlCo-type alloys characterized by ΔS_M values between -7.6 and -9.4 J/kg K, $\mu_o\Delta H = 5$ T, and RC 413–679 J/kg, but low Curie temperatures, typically well below 100 K (which constrains refrigerant applications to such temperature intervals) [11] or HoDyAlCo systems with ΔS_M of up to -11.7 J/kg K, $\mu_o\Delta H = 5$ T, RC = 365 J/kg and $T_C = 17$ K [12].

An ample group of materials which has been extensively studied for MCE applications are La-based manganites with perovskite structure, because of their competitive cost of production, chemical stability and easy tailoring of magnetic properties [2, 4]. In fact, a significant number of compositional variations have been explored for $LaMnO_3$-type manganites, including cations with 2+ *or* 1+ valence states, such as LaSr, LaCa, LaBa, LaPb, LaNd, LaY, LaLi, and La(Na,K,Ag), among others [4, 13–16]. However, reports concerning the effect of concomitant cations with mixed-valence 2+ *and* 1+ on La-based manganites are much less numerous [2, 4]. In this work, we present a systematic study on the effect of the progressive replacement of Ag^{1+} and Sr^{2+} cations on the MCE of $La_{0.80}(Ag_{1-x}Sr_x)_{0.20}MnO_3$ manganites.

Experimental techniques

Mixed-valence polycrystalline $La_{0.80}(Ag_{1-x}Sr_x)_{0.20}MnO_3$ manganites ($x = 0.0$, 0.25, 0.50, 0.75, 1.0) were synthesized by means of the solid-state reaction method. Details on the synthetic procedure are described elsewhere [17]. Chemical composition across the compositional series was verified by means of X-ray photoelectron spectroscopy in a VG Microtech Multilab ESCA2000 coupled with a CLAM4 MCD detector with Al-K_α radiation. The elemental chemical analysis was carried out by means of deconvolution of the core-level signals of the XPS spectra. This deconvolution process involves the removal of the background by Shirley method [18, 19]. Then, we calibrate the binding energy (BE) with reference materials (La_2O_3, $SrCO_3$, Mn_3O_4, and AgO) for which we propose Gaussian–Lorentzian curves with spectroscopic criteria and the sensitivity relative factors reported by Scofield [20]. The fitting of the XPS spectra was performed with the program SDP v4.1 [21]. Magnetization measurements were performed by means of a Physical Property Measuring System equipped with the vibrating sample magnetometer module (PPMS-9T Evercool I, Quantum Design platform). The isothermal magnetic entropy change as a function of temperature $\Delta S_M(T)$ was calculated from a set of magnetization isotherms measured each 5 K over the temperature interval 200–400 K. The maximum applied magnetic field change $\mu_o\Delta H_{max}$ was of 5.0 T. The magnetic entropy variation ΔS_M was calculated through the numerical integration of the Maxwell relation [2, 4]:

$$\Delta S_M(T) = \int_o^{B_{max}} \left(\frac{\partial M}{\partial T}\right)_B dB. \quad (1)$$

Results

Details on phase distribution analysis by powder X-ray technique are given in [17], for which the solid solution $La_{0.80}(Ag_{1-x}Sr_x)_{0.20}MnO_3$ across the compositional series was identified together with minor secondary phases Mn_3O_4 and metallic Ag for the sample with $x = 0.0$. Decreasing peak intensities of the secondary phases was observed as the Sr concentration increases, with no detectable presence of Ag or Mn_3O_4 for the $La_{0.80}Sr_{0.20}MnO_3$ sample. Very similar phase distribution has been previously described in equivalent $La_{1-x}Ag_xMnO_3$ manganites [22–24].

A central issue for the correlation between chemical composition variation and magnetic properties of La-based manganites is the relative amount of Mn^{4+} and Mn^{3+} ions present in each sample, as will be described within the "Discussion" section. Firstly, we confirm the Mn divalent state in our samples by the splitting of the Mn 3s core-level signal of the XPS spectra corresponding to the $La_{0.80}(Ag_{0.25}Sr_{0.75})_{0.20}MnO_3$ manganite as example (Fig. 1a). The linear relation between the Mn valence and the exchange splitting energy has been described in [25, 26]. As a second step, we quantify the content of Mn^{4+}–Mn^{3+} cations by using the XPS high-resolution spectra of the core-level energies for the Mn $2p_{1/2}$ and Mn $2p_{3/2}$, for which Fig. 1b displays such core levels for the $La_{0.80}(Ag_{0.50}Sr_{0.50})_{0.20}MnO_3$ manganite as example, together with the same Mn 2p transition for all the compositions (inset). These core-level signals were used to

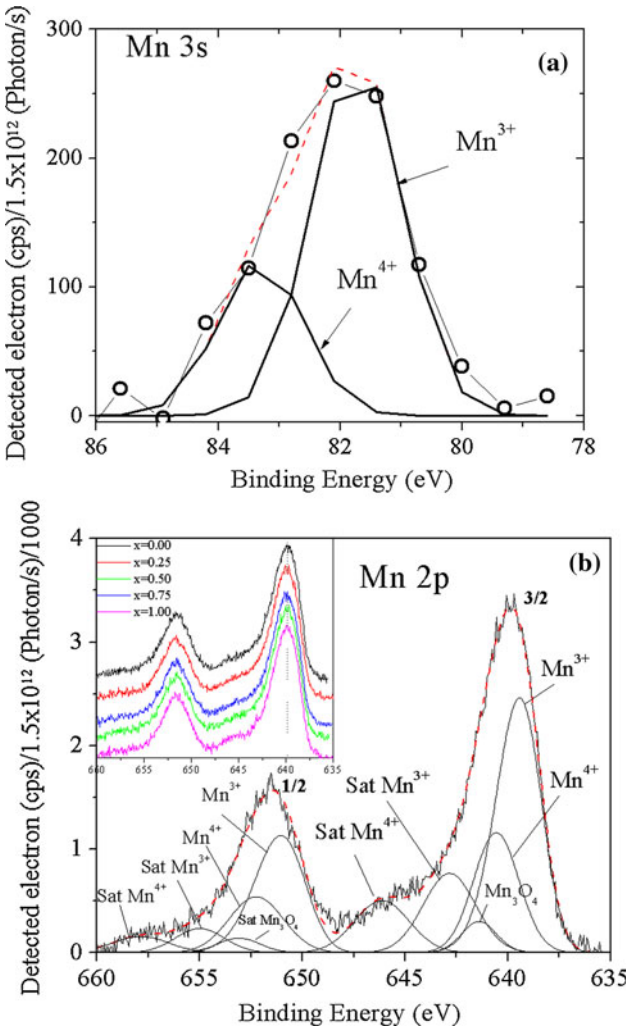

Fig. 1 **a** Experimental XPS spectra (*circles*) of the Mn 3s core-level for the $La_{0.80}(Ag_{0.25}Sr_{0.75})_{0.20}MnO_3$ manganite. The fitting of the signal (*dashed line in red*) was carried out with peaks (*continuous lines*) associated with Mn^{3+} and Mn^{4+} cations. **b** High resolution XPS spectra of the Mn 2p core-level for the $La_{0.80}(Ag_{0.50}Sr_{0.50})_{0.20}MnO_3$ manganite. The fitting of the signal is shown as *dashed line in red*. The *inset* shows the Mn 2p spectra for the whole compositional series (Color figure online)

calculate the Mn^{4+}–Mn^{3+} content by means of a deconvolution process using the peaks located at the following BE: (a) For the Mn $2p_{3/2}$ core-level, peaks at BE = 639.43 eV and its satellite at 642.84 eV, both corresponding to Mn^{3+}, while peaks at 640.56 eV and its satellite at 646.13 eV correspond to Mn^{4+}, (b) For the Mn $2p_{1/2}$ core-level, peaks at 651.05 eV and its satellite at 655.00 eV, both corresponding to Mn^{3+}, while peaks at 652.25 eV and its satellite at 657.88 eV correspond to Mn^{4+}. This assignment of peaks and satellites for Mn^{3+} and Mn^{4+} cations based on the same Mn $2p_{1/2}$ and Mn $2p_{3/2}$ core levels has been proposed in [27] for equivalent kind of perovskites, studied for catalysis applications. The Mn^{4+} content shown in Table 1 exhibits an

Table 1 XPS elemental composition (at%) of Mn^{3+} and Mn^4 atoms for the manganite series $La_{0.80}(Ag_{1-x}Sr_x)_{0.20}MnO_3$, according to the deconvolution analysis of Fig. 1

x	Mn^{3+}	Mn^{4+}	Ag^{1+}	Ag^0
0.0	64.1	29.1	2.4	0.5
0.25	61.0	33.8	1.9	0.4
0.50	62.3	33.1	1.7	0.4
0.75	60.9	34.7	0.5	0.2
1.0	60.2	37.4	0.00	0.00

This deconvolution process was carried out by using the peaks located at the following binding energies (BE): (a) For the Mn $2p_{3/2}$ core-level, peaks at BE = 639.43 eV and its satellite at 642.84 eV, both corresponding to Mn^{3+}, while peaks at 640.56 eV and its satellite at 646.13 eV correspond to Mn^{4+} ,(b) For the Mn $2p_{1/2}$ core-level, peaks at 651.05 eV and its satellite at 655.00 eV, both corresponding to Mn^{3+}, while peaks at 652.25 eV and its satellite at 657.88 eV correspond to Mn^{4+}. For Ag atoms we used the core-level signal of Ag 3d ($3d_{5/2}$: 367.03 eV for Ag^{1+} and 368.20 eV for Ag^0) ([17])

increasing tendency with increasing Sr content x as a result of the oxidation of Mn^{3+} atoms to compensate the charge of the incorporated Sr^{2+} ions. These values are consistent with those obtained by other experimental techniques such as redox titrations reported for equivalent $La_{0.80}Sr_{0.20}MnO_3$ manganites (with Mn^{4+} content of 34.0 at% for the $La_{0.80}Sr_{0.20}MnO_3$ manganite [28]) as well as for equivalent $La_{0.7}Sr_{0.3-x}Ag_xMnO_3$ (x values upto 0.2) with Mn^{4+} content between 29.5 and 34.5 at% for similar Ag concentrations [24]. Complementary, the Mn concentration of the Mn_3O_4 phase was evaluated by means of the Mn $2p_{3/2}$ and Mn $2p_{1/2}$ core levels and the peaks located at BE = 641.40 eV and 653.10 eV, respectively. For this phase, the following concentrations (% elemental) were determined: 6.8, 5.2, 4.6, 4.4, 2.4 for the samples $x = 0.0$, 0.25, 0.50, 0.75, and 1.0, respectively. This decreasing amount of Mn_3O_4 with increasing Sr content confirms the tendency observed by XRD results [17], except of the $x = 1.0$ sample, for which XPS indicates that Mn_3O_4 is still forming at a small fraction of 2.4 %. Such fraction is below the XRD detection limit, and thus it was not recorded in the corresponding X-ray diffractogram. For the silver concentration we found two oxidation states for Ag atoms, one associated to Ag^0 (metallic) with BE = 368.20 eV corresponding to the Ag $3d_{5/2}$ core-level, and the other to Ag^{1+} for the BE = 367.03 eV for the same core-level. The presence of Ag^{1+} confirms the incorporation of Ag atoms within the crystal unit cell of the $La(AgSr)MnO_3$ manganites, while the vanishing content of metallic silver (Table 1) is also consistent with XRD results [17]. No silver atoms were detected for $x = 1.0$. Details for the Ag composition procedure from the deconvolution of the Ag 3d core-level signal are described in [17, 27, 29].

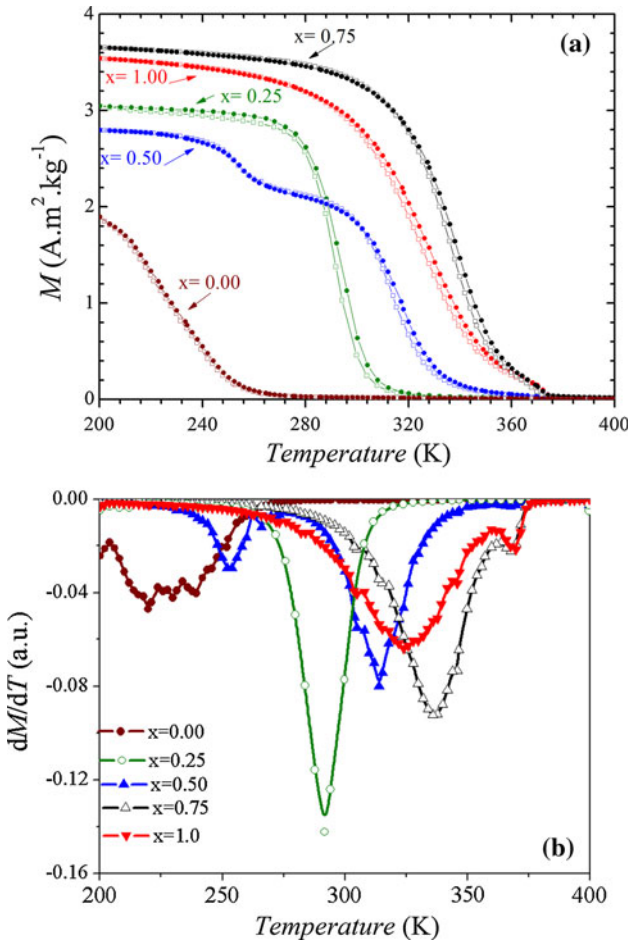

Fig. 2 **a** Thermomagnetization $M(T)$ curves for the $La_{0.80}(Ag_{1-x}Sr_x)_{0.20}MnO_3$ manganite series under field cooled (FC, *open symbols*) and field heating (FH, *full symbols*) regimes. The applied magnetic field was fixed at 5 mT for all the samples, **b** dM/dT curves as a function of temperature for T_C determination

Concerning magnetic properties, thermomagnetization $M(T)$ curves under field cooled and field heating regimes for an applied low magnetic field of 5 mT are displayed in Fig. 2a for the $La_{0.80}(Ag_{1-x}Sr_x)_{0.20}MnO_3$ manganite series. All the curves display a decreasing behavior with increasing temperature as the magnetic order–disorder transition approaches. A small thermal hysteresis (of up to $\Delta T = 3$ K) is manifested for the manganites with $x > 0.0$. For the $x = 0.50$ sample, a step is observed on its corresponding $M(T)$ plot between 250 and 260 K, which can be attributed to a second phase present in a volume fraction below the detection limit of the XRD technique ($\sim$4 %). This phase probably corresponds to $SrMnO_3$, with $T_C = 260$ K [30], which can remain as an intermediate product of the reaction during the formation of $La_{1-x}Sr_xMnO_3$ manganites [31]. A subtle, much less defined step in the $M(T)$ curve within the interval 364–374 K is also visible for the $x = 0.75$ and 1.0 samples [see Fig. 2a], likely corresponding to the marginal secondary phase $La_{2/3}Sr_{1/3}MnO_3$ ($T_C = 368$ K [2, 4]), which could be segregated during the formation of $La_{1-x}Sr_xMnO_3$ manganites [31]. According to the thermomagnetization data of Fig. 2a, this phase should have a volume fraction around 4.0 %, which is at the threshold detection of the XRD technique. The Curie temperatures for all the $La_{0.80}(Ag_{1-x}Sr_x)_{0.20}MnO_3$ compounds were taken at the inflexion point of each curve [Fig. 2b]. T_C determined from Fig. 2b showed an increasing tendency with increasing Sr content x up to $x = 0.75$ (from 225 K at $x = 0.0$ upto 336 K at $x = 0.75$), followed by a noticeable reduction at $x = 1.0$ ($T_C = 324$ K). The well defined peak at the magnetic transition observed for all manganites with $x > 0.0$ reflects a good chemical homogeneity, in contrast with the $La_{0.80}Ag_{0.20}MnO_3$ sample. The magnetic transition temperature of the secondary Mn_3O_4 phase is not visible in Fig. 2 because such temperature is far below 200 K ($\sim$43 K [32]). The tendency observed for T_c is in agreement with previous reports concerning equivalent $La_{0.7}Sr_{0.3-x}Ag_xMnO_3$ manganites [24].

Isothermal magnetization curves up to $\mu_oH_{max} = 5$ T at variable temperature for selected compositions of the manganites series $La_{0.80}(Ag_{1-x}Sr_x)_{0.20}MnO_3$ ($x = 0.0,0.50,1.0$) are displayed in Fig. 3. The transition from ferromagnetic to paramagnetic ordering (i.e., nearly linear-like $M(\mu_oH)$ is visible for decreasing temperature for all the samples. No marked deviations were observed for the low-field (<1.0 T) $M(\mu_oH)$ curves across the compositional series, which is indicative of the absence of metamagnetic-like transitions [33]. Very similar behavior of the isothermal magnetization was reported for equivalent $LaAgMnO_3$ manganites prepared by the same method [23, 24]. Arrott plots M^2 versus μ_oH/M for selected compositions are shown in Fig. 4 ($x = 0.25,0.75$). The positive slope observed for these plots is indicative of a ferromagnetic–paramagnetic transition of second-order character [34] and is in agreement with previous reports on equivalent $La_{0.7}Sr_{0.3-x}Ag_xMnO_3$ manganites [24].

The magnetic entropy variations $|\Delta S_M|$ as a function of temperature, calculated at variable $\mu_o\Delta H_{max}$ from 1 to 5 T, are displayed in Fig. 5a for the $La_{0.80}(Ag_{0.75}Sr_{0.25})_{0.20}MnO_3$ manganite. These magnetic entropy plots show single-peak behavior across the temperature interval, with $|\Delta S_M^{peak}|$ values having an increasing tendency with increasing $\mu_o\Delta H$. For $\mu_o\Delta H = 5.0$ T, an interesting maximum of 4.6 J/kgK is observed, which is comparable with the $|\Delta S_M^{peak}| = 5.6$ J/kg K of pure Gd at $\mu_o\Delta H = 2.0$ T [35]. Additionally, an interval of temperature at the full-width at half maximum of the $\Delta S_M(T)$ curve (denoted as $\delta T_{FWHM} = T_{hot} - T_{cold}$) of 35 K is observed for $\mu_o\Delta H = 2.0$ T with $|\Delta S_M^{peak}| = 2.4$ J/kg K, which is important for establishing wide thermodynamic cycles for the magnetic cooling process.

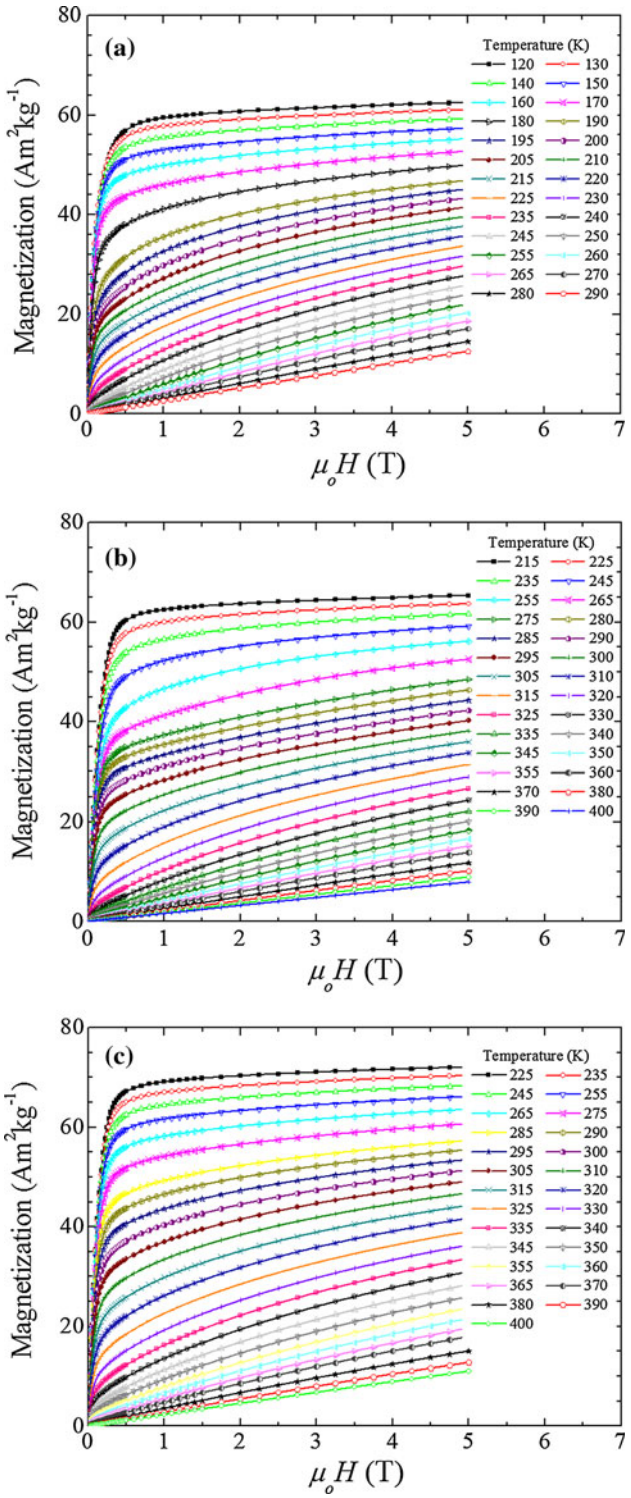

Fig. 3 Isothermal magnetization curves up to $\mu_o H_{max} = 5$ T for the manganite samples **a** $La_{0.80}Ag_{0.20}MnO_3$, **b** $La_{0.80}(Ag_{0.50}Sr_{0.50})_{0.20}MnO_3$, and **c** $La_{0.80}Sr_{0.20}MnO_3$

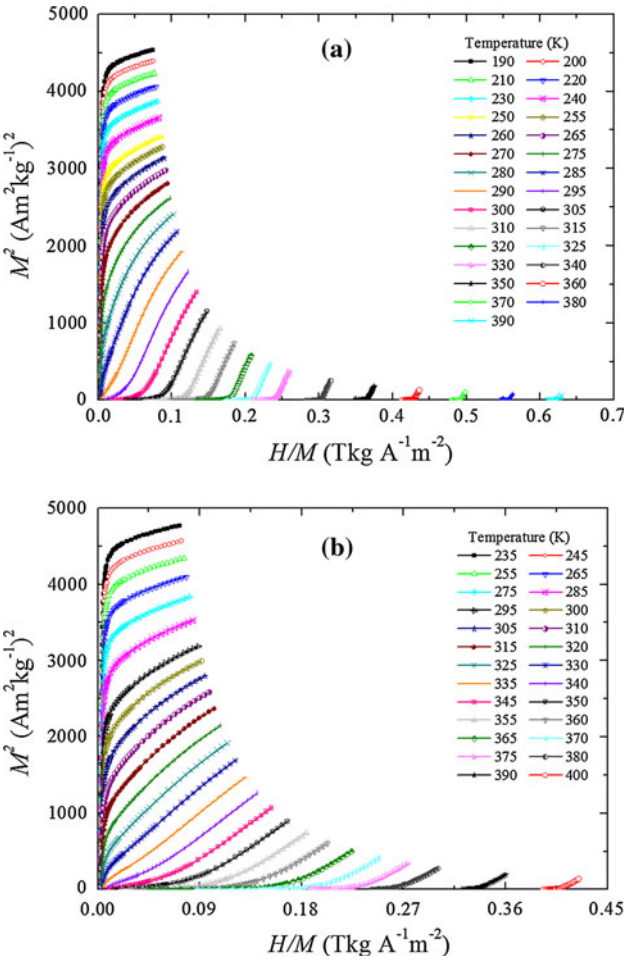

Fig. 4 *Arrott plots* for the manganite samples **a** $La_{0.80}(Ag_{0.75}Sr_{0.25})_{0.20}MnO_3$ and **b** $La_{0.80}(Ag_{0.25}Sr_{0.75})_{0.20}MnO_3$

Complementary, the *RC* has been calculated by means of the three established criteria used in literature: (a) $|\Delta S_M^{peak}|$ x δT_{FWHM} (denoted hereafter as *RC*-1). Here, δT_{FWHM} coincides with the temperature interval of the thermodynamic cycle; (b) calculating the integral, under the $\Delta S_M(T)$ curves between T_{hot} and T_{cold} (hereafter denoted as *RC*-2, i.e., $RC-2 = \int_{T_{hot}}^{T_{cold}} [\Delta S_M(T)]_{\Delta B} dT$), and (c) maximum $|\Delta S_M|$ x δT^{RC-3} product under the $\Delta S_M(T)$ curve (labeled as *RC*-3; in this case, the temperature interval define different hot and cold temperatures which are been labeled as T_{hot}^{RC-3} and T_{cold}^{RC-3}) [36]. The field dependence of the RC values for the $La_{0.80}(Ag_{0.75}Sr_{0.25})_{0.20}MnO_3$ manganite are shown in Fig. 5b. A maximum *RC*-1 of 215 J/kg was observed at $\mu_o \Delta H = 5.0$ T. For the manganites corresponding to $x = 0.75$ and 1.0, equivalent behavior was observed for both $|\Delta S_M|$ and refrigerant capacities, with maximum values of 3.4 J/kg K and 275 J/kg and 3.1 J/kg K and 304 J/kg, respectively. Results of the magnetocaloric parameters of the series studied are summarized in Table 2. Similar magnetic entropy variation has been reported in equivalent $La_{1-x}Ag_xMnO_3$ manganites by means of isothermal magnetization curves [22, 23] and by heat capacity measurements [37]

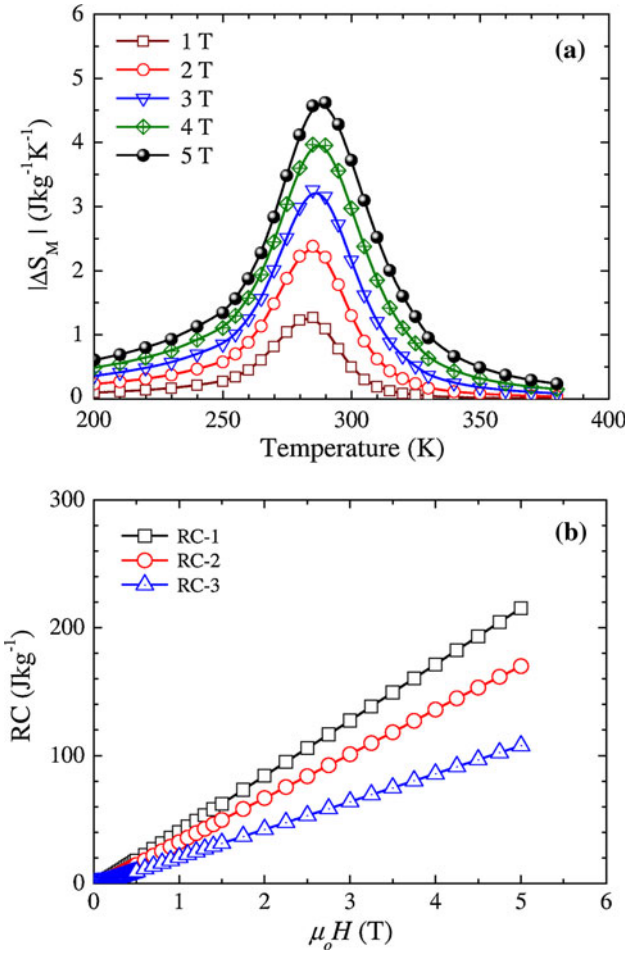

Fig. 5 **a** Temperature dependence of the magnetic entropy change $|\Delta S_M(T)|$ and **b** magnetic field dependence of the refrigerant capacity values for the $La_{0.80}(Ag_{0.75}Sr_{0.25})_{0.20}MnO_3$ manganite

and for equivalent $La_{0.7}Sr_{0.3-x}Ag_xMnO_3$ (x values upto 0.2) [24].

In addition, the magnetic entropy variation calculated up to $\mu_o\Delta H = 5.0$ T for the $La_{0.80}(Ag_{0.50}Sr_{0.50})_{0.20}MnO_3$ manganite is shown in Fig. 6, for which a double-peak behavior is manifested due to the contribution of the $SrMnO_3$ secondary phase. For this sample, very larger *RC*-2 values of 239 and 94 J/kg were recorded for $\mu_o\Delta H = 5.0$ and 2.0 T, respectively (Table 2), together with a large δT_{FWHM} as high as 101 K at $\mu_o\Delta H = 2.0$ T and 110 K at $\mu_o\Delta H = 5.0$ T, respectively. This wide δT_{FWHM} has the additional advantage of embracing temperature intervals around 300 K ($265 \leq T \leq 312$ K), which renders this specific composition as potential candidate for room temperature magnetic refrigeration devices. A similar behavior of the $|\Delta S_M|$ curve was observed for the manganite corresponding to $x = 0.0$, with a remarkable δT_{FWHM} of 113 K at $\mu_o\Delta H = 5.0$ T. Unlike the $x = 0.50$ sample, both T_{hot} and T_{cold} temperatures for the $x = 0.0$ manganite are well below 300 K. Results are summarized in Table 2.

Discussion

From a fundamental viewpoint, the electronic properties of mixed-valence perovskites relies to a significant extent on the double-exchange interaction, which is afforded by the conversion of Mn^{3+} cations into Mn^{4+} ions upon doping the original $LaMnO_3$ compound with divalent or monovalent cations [38]. On the basis of the electronic configuration of Mn^{3+} ($t_{2g}^3e_g^1$) and Mn^{4+} ($t_{2g}^3e_g^0$), it can be elucidated that the presence of Mn^{4+} ions allow the

Table 2 Peak magnetic entropy change $|\Delta S_M^{peak}|$, *RC-1*, *RC-2*, δT_{FWHM}, T_{hot}, T_{cold}, *RC-3*, δT^{RC-3}, and T_{hot}^{RC-3} and T_{cold}^{RC-3} related to *RC-3* for the $La_{0.80}(Ag_{1-x}Sr_x)_{0.20}MnO_3$ manganites series ($0.00 \leq x \leq 1.00$)

x	0.00		0.25		0.50		0.75		1.00	
	$\mu_o\Delta H_{max}$ (T)		$\mu_o\Delta H_{max}$ (T)		$\mu_o\Delta H_{max}$ (T)		$\mu_o\Delta H_{max}$ (T)		$\mu_o\Delta H_{max}$ (T)	
	2 T	5 T	2 T	5 T	2 T	5 T	2 T	5 T	2 T	5 T
$\|\Delta S_M^{peak}\|$ (Jkg^{-1} K^{-1})	1.1	2.3	2.4	4.6	1.3	2.8	1.5	3.4	1.4	3.1
RC-1(Jkg^{-1})	107	266	84	215	129	309	108	275	117	304
RC-2 (Jkg^{-1})	86	220	67	170	94	239	85	215	92	238
δT_{FWHM} (K)	97	113	35	47	101	110	70	80	84	96
T_{hot} (K)	247	259	301	312	328	338	352	362	346	356
T_{cold} (K)	150	146	266	265	227	228	282	282	262	260
RC-3 (Jkg^{-1})	57	142	42	108	75	172	54	138	59	152
δT^{RC-3} (K)	79	86	33	45	75	84	66	78	76	97
T_{hot} (K)*	239	248	300	311	318	327	351	361	343	356
T_{cold} (K)*	160	162	267	266	243	243	285	283	267	259

All of them are given for a magnetic field change of $\mu_o\Delta H_{max}$ of 2 and 5 T

* Related to RC-3

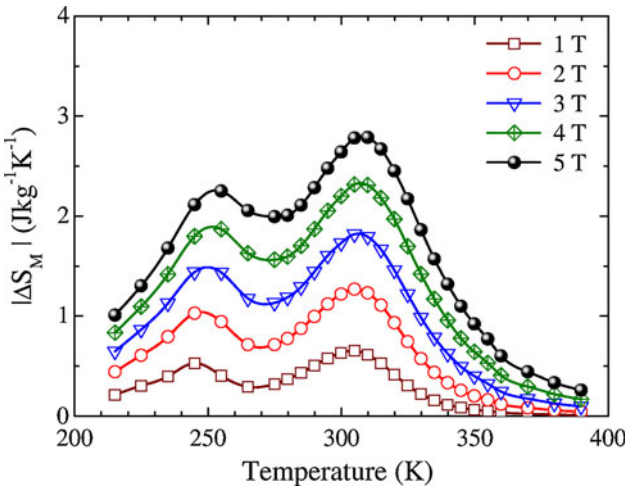

Fig. 6 Temperature dependence of the magnetic entropy change $|\Delta S_M(T)|$ for the $La_{0.80}(Ag_{0.50}Sr_{0.50})_{0.20}MnO_3$ manganite

hopping of e_g electrons of Mn^{3+} to neighboring Mn^{4+} through double-exchange interaction, which in turn mediates ferromagnetic ordering and electronic conduction [38]. Hence, the increasing tendency of the Curie temperature observed for manganites with Sr contents upto $x = 0.75$ is consistent with the increasing Mn^{3+} to Mn^{4+} relative proportions which is reported in Table 1.

A complementary aspect that influences the electronic properties of these kinds of perovskites is the lattice effects caused by doping with 2+ or 1+ cations of different ionic radius, in particular, the variation of the Mn–O–Mn bond angle [38–40]. In this sense, an important criterion for analyzing the crystal structure of perovskite ABO_3 compounds (where A corresponds to a trivalent or divalent cation and B corresponds to Mn for the case of manganites) is the tolerance factor t, which represents the capacity of the perovskite structure to accept A and B ions that allows dodecahedral and octahedral coordination, respectively [38, 40]. Stable crystal structures have representative t values as follows: for the ideal cubic perovskite $t = 1.0$, while for the interval $0.9 < t < 1.0$, the unit cell presents a rhombohedral distortion. For $t < 0.9$ the structure becomes orthorhombic [40]. In order to quantify t, the following Equation has been established [38, 40]:

$$(r_A + r_O) = t \cdot \sqrt{2}(r_{Mn} + r_O) \quad (2)$$

where r_A, r_O, r_{Mn} stand for the ionic radii of the cations A, O, and Mn, respectively.

For the present case, and bearing in mind the size and oxidation states of the cations involved ($r_{La3+} = 1.50$ Å, $r_{Ag+} = 1.42$ Å $r_{Sr2+} = 1.58$ Å, $r_{Mn3+} = 0.72$ Å, $r_{Mn4+} = 0.67$ Å, and $r_{O2-} = 1.26$ Å [41]), we propose the following expressions for the mean radii $\langle r_A \rangle$ and $\langle r_B \rangle$ for our $La_{0.80}(Ag_{1-x}Sr_x)_{0.20}MnO_3$ phases:

$$\langle r_A \rangle = r_{La^{3+}}(0.80) + r_{Ag^+}(1-x)(0.20) + r_{Sr^{2+}}(x)(0.20) \quad (3)$$

$$\langle r_B \rangle = r_{Mn^{4+}}(1-x)(0.20) + r_{Mn^{4+}}(x)(0.40) + r_{Mn^{3+}}(1-[(1-x)(0.20) + (x)(0.40)]). \quad (4)$$

By inserting the experimental Mn^{3+}, Mn^{4+}, and Ag^{1+} atomic contents of Table 1 into Eqs. 2, 3, and 4, the resulting plots are shown in Fig. 7a. The r_A increases up to x = 0.75 as a consequence of the progressive incorporation of large Sr cations into the crystal structure containing Ag atoms. For $x = 1.0$, r_A decreases due to the absence of Ag atoms. The same r_A tendency was described by Rietveld analysis in equivalent $La_{0.7}Sr_{0.3-x}Ag_xMnO_3$ manganites [24]. In contrast, r_B remains constant across the compositional series. In addition, the tolerance factor t (Fig. 7b) exhibits an increasing behavior up to the Sr content $x = 0.75$, reflecting the tendency to a more cubic-like structure with Mn–O–Mn angles (Θ) becoming closer to 180°. The augmenting Θ angles favors DE interaction, which leads to the progressive improvement of T_C observed in Fig. 2 [38, 39]. The reduced t observed at $x = 1.0$

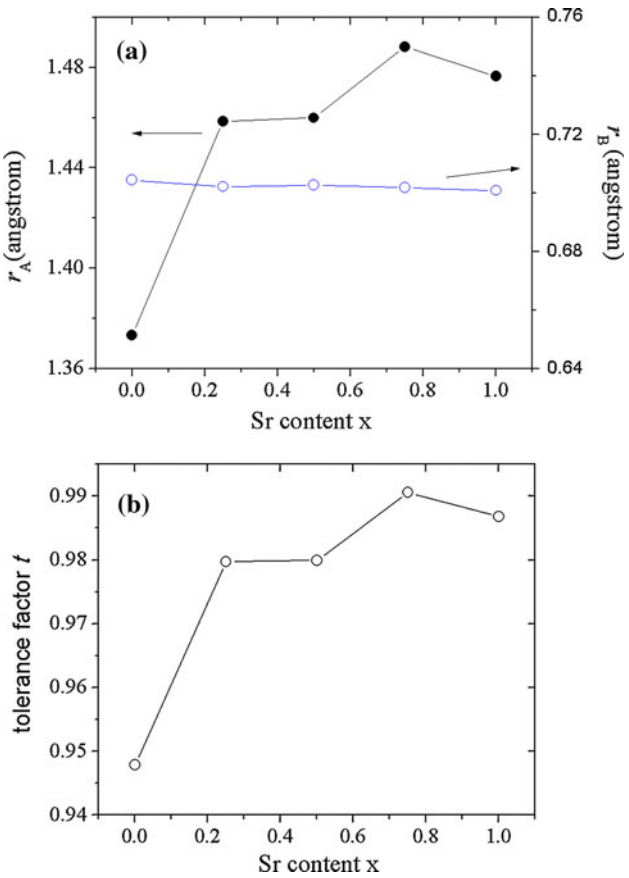

Fig. 7 Ionic radius for the A-site, r_A and the B-site, r_B (**a**), and tolerance factor of the perovskite structure ABO_3 (**b**) as a function of the Sr content in $La_{0.80}(Ag_{1-x}Sr_x)_{0.20}MnO_3$ manganites series

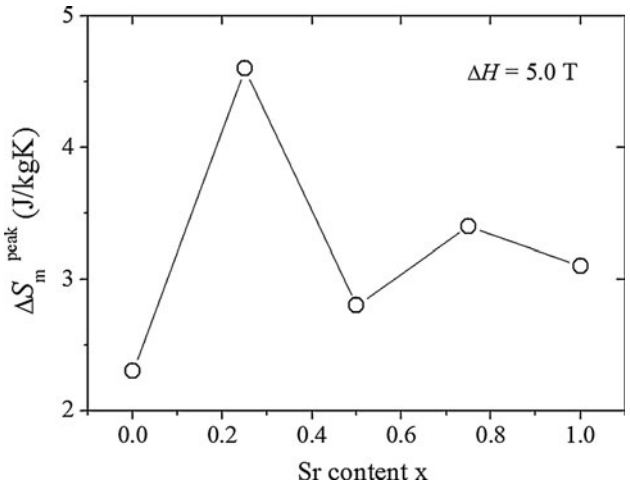

Fig. 8 Peak magnetic entropy values $|\Delta S_M^{peak}|$ as a function of the Sr content for the $La_{0.80}(Ag_{1-x}Sr_x)_{0.20}MnO_3$ manganites series ($\mu_o\Delta H = 5.0$ T)

implies a more distorted crystal structure compared with $x = 0.75$, which affects the DE yielding reduced Curie transitions. This correlation between structural variation and magnetic properties has been described with profusion in similar La-based manganites [38, 39].

The enhancement of the DE interaction also benefits the MCE performance of the $La_{0.80}(Ag_{1-x}Sr_x)_{0.20}MnO_3$ manganites series, since improved DE favors higher magnetizations and steeper *M(T)* curves at the Curie transition, both of which have a beneficial effect on the magnetocaloric parameter $|\Delta S_M^{peak}|$. According to Eq. (1), $|\Delta S_M|$ is directly influenced by d*M*/d*T*. Thus, following the derivatives shown in Fig. 2b, a maximum in $|\Delta S_M|$ should manifest for the $x = 0.25$ sample having the highest slope with well defined shape at the Curie transition, together with a marked reduction for $x = 1.00$ with a significantly reduced steep at T_C and intermediate values for the remaining compositions. This tendency is confirmed in Fig. 8 for peak magnetic entropy values $|\Delta S_M^{peak}|$ as a function of the Sr content x for $\mu_o\Delta H = 5$ T, for which the noticeable enhancement of $|\Delta S_M^{peak}| = 4.6$ J/kg K observed at $x = 0.25$ is consistent with the pronounced steep of its corresponding *M(T)* curve at the Curie point.

Conclusion

Mixed-valence $La_{0.80}(Ag_{1-x}Sr_x)_{0.20}MnO_3$ manganites with concomitant Ag^{1+} and Sr^{2+} ions were successfully synthesized by the solid-state reaction method. The mixed-valence and content of Mn cations were verified by means of XPS technique, which indicated an increasing number of Mn^{4+} ions with increasing Sr content up to $x = 0.75$. The MCE parameters ($|\Delta S_M^{peak}|$, *RC*, δT_{FWHM}) showed a clear dependence with the Sr content as a consequence of the progressive improvement of the double-exchange interaction promoted by the increasing Mn^{4+} cations and the tolerance factor. Maximum $|\Delta S_M|$ of 4.6 J/kgK was obtained for the $La_{0.80}(Ag_{0.75}Sr_{0.25})_{0.20}MnO_3$ manganite at $\mu_o\Delta H = 5.0$ T.

Acknowledgments I. Betancourt acknowledges financial support from research project UNAM-PAPIIT IN104310. M.E. Amano is grateful for the scholarship received from UNAM-PAPIIT IN104310 and CONACYT-82358 research grants. J.L. Sanchez Llamazares acknowledges the financial support received from CONACYT, Mexico, under project CB-2010-01-156932. Support received from Laboratorio Nacional de Investigaciones en Nanociencias y Nanotecnología (LINAN, IPICYT) is kindly acknowledged. C.F.S.V. thanks CSIC, Spain, for the Ph.D. grant received (JAEPRE-08-00508).

References

1. Giauque WF, MacDougall DP (1993) Phys Rev 43:768–771
2. Tishin AM, Spichkin YE (2003) The Magnetocaloric Effect and its Applications. Institute of Physics, Bristol-Philadelphia
3. Brück E, Tegus O, Li XW, de Boer FR, Buschow KHJ (2003) Phys B 327:431–435
4. Phan MH, Yu SC (2007) J Magn Magn Mater 308:325–340
5. Canepa F, Cirafici S, Napoletano M, Ciccarelli C, Belfortini C (2005) Solid State Commun 133:241–246
6. Tegus O, Bruck E, Buschow KHJ, de Boer FR (2002) Nature 415:150–155
7. Tegus O, Fuquan B, Dagula W, Zhang L, Brück E, Si PZ, de Boer FR, Buschow KHJ (2005) J Alloys Compd 396:6–10
8. Rama Rao NV, Gopalan R, Chandraekaran, Suresh VKJ (2009) J Alloys Compd 478:59–64
9. Ma SC, Cao QQ, Xuan HC, Zhang CL, Shen LJ, Wang DH, Du YW (2011) J Alloys Compd 509:1111–1115
10. Sánchez Llamazares JL, Garcia C, Hernando B, Prida VM, Baldomir D, Serantes D, Gonzalez J (2011) Appl Phys A 103:1125–1129
11. Luo Q, Wang WH (2010) J Alloys Compd 495:209–2014
12. Liang L, Hui X, Zhang CM, Lu ZP, Chen GL (2008) Solid State Commun 146:49–53
13. Hwang HY, Cheong SW, Radaelli PG, Marezio M, Batlogg B (1995) Phys Rev Lett 75:914–918
14. Yu JY, Zhang SY, Liu GH, Wu HY, Wang L (2007) Solid State Commun 142:333–337
15. Sdiri N, Bejar M, Dhahri E (2007) J Magn Magn Mater 311:512–516
16. Cheikh-Rouhou Koubaa W, Koubaa M, Cheikhrouhou A (2009) Phys Procedia 2:989–995
17. Amano ME, Betancourt I, Huerta L (2013) J Am Ceram Soc 96:812–815
18. Castle JE, Salvi AM (2001) J Vac Sci Technol A 19:1170–1177
19. Vegh J (2006) J Electron Spectrosc 151:159–164
20. Scofield H (1956) J Elect Spect Related Phenom 8:129–133
21. SDP v4.1 (32 bit) Copyright © 2004, XPS International, LLC, Compiled January 17 (2004)
22. Tang T, Gu KM, Cao QQ, Wang DH, Zhang SY, Du YW (2000) J Magn Magn Mater 222:110–114
23. The Hien N, Phu Thuy N (2002) Phys B 319:168–173
24. Cheikh-Rouhou Koubaa W, Koubaa M, Cheikhrouhou A (2008) J Alloy Compd 453:42–48
25. Galakhov VR, Demeter M, Bartkowski S, Neumann M, Ovechkina NA, Kurmaev EZ, Logachevskaya NI, Mukovskii YM, Mitchell J, Ederer DL (2002) Phys Rev B 65:113102–113105

26. Beyreuther E, Grafström S, Eng LM, Thiele C, Dörr K (2006) Phys Rev B 73:155425
27. Kucharczyk B, Tylus B (2008) Appl Catal A-Gen 335:28–36
28. Mahesh R, Mahendiran R, Raychaudhuri AK, Rao CNR (1995) J Sol Stat Chem 114:297302
29. Wei Z-X, Weia L, Gong L, Wang Y, Hu C-W (2010) J Hazard Mater 177:554–560
30. Choi Y, Yoo YZ, Chmaissen O, Ullah A, Kolesnik S, Kimball CW, Haskel D, Jiang JS, Bader SD (2007) Appl Phys Lett 91:022503
31. Uskokovic V, Drofenik M (2006) Mater Sci Forum 518:119–125
32. Si PZ, Li D, Choi CJ, Li YB, Geng, Zhang ZD (2007) Solid State Commun 142:723–727
33. Bingham NS, Phan MH, Srikanth H, Torija MA, Leigthon C (2009) J Appl Phys 106:023909
34. Banerjee BK (1964) Phys Lett 12:16–20
35. Dan'kov SY, Tishin AM, Pecharsky VK, Gschneidner KA (1998) Phys Rev B 57:3478–3484
36. Sanchez Llamazares JL, Flores-Zuñiga H, Sanchez-Valdes C, Ross CA, Garcia C (2012) J Appl Phys 111:932–936
37. Kamilov IK, Gamzatov AG, Aliev AM, Batdalov AB, Aliverdiev AA, Abdulvagidov ShB, Melnikov OV, Gorbenko OYu, Kaul AR (2007) J Phys D 40:4413–4417
38. Coey JMD, Viret M, Von Molnar S (1999) Adv Phys 48:167–180
39. Tokura Y (2006) Rep Prog Phys 69:797–815
40. Attfield JP (1998) Chem Mater 10:3239–3255
41. Shannon RD (1976) Acta Cryst A 32:751–761